Acta Crystallographica Section D
Biological Crystallography
ISSN 0907-4449

Mutations inducing an active-site aperture in *Rhizobium* sp. sucrose isomerase confer hydrolytic activity

Alexandra Lipski,[a] Hildegard Watzlawick,[b] Stéphanie Ravaud,[a]‡ Xavier Robert,[a] Moez Rhimi,[a] Richard Haser,[a] Ralf Mattes[b] and Nushin Aghajari[a]*

[a]Laboratory for Biocrystallography and Structural Biology of Therapeutic Targets, Molecular and Structural Bases of Infectious Diseases, UMR 5086 CNRS and University of Lyon, 7 Passage du Vercors, F-69367 Lyon CEDEX 07, France, and [b]Institut für Industrielle Genetik, Universität Stuttgart, Allmandring 31, D-70569 Stuttgart, Germany

‡ Present address: Institut de Biologie Structurale, University of Grenoble 1, CEA, CNRS, 41 Rue Jules Horowitz, F-38027 Grenoble CEDEX 1, France.

Correspondence e-mail: nushin.aghajari@ibcp.fr

Received 17 September 2012
Accepted 4 November 2012

PDB References: sucrose isomerase, R284C mutant, 4h2c; soaked with deoxynojirimycin, 4gin; F164L mutant, soaked with glucose, 4gi6; soaked with sucrose, 4gi8; soaked with isomaltulose, 4gia; soaked with trehalulose, 4gi9

Sucrose isomerase is an enzyme that catalyzes the production of sucrose isomers of high biotechnological and pharmaceutical interest. Owing to the complexity of the chemical synthesis of these isomers, isomaltulose and trehalulose, enzymatic conversion remains the preferred method for obtaining these products. Depending on the microbial source, the ratio of the sucrose-isomer products varies significantly. In studies aimed at understanding and explaining the underlying molecular mechanisms of these reactions, mutations obtained using a random-mutagenesis approach displayed a major hydrolytic activity. Two of these variants, R284C and F164L, of sucrose isomerase from *Rhizobium* sp. were therefore crystallized and their crystal structures were determined. The three-dimensional structures of these mutants allowed the identification of the molecular determinants that favour hydrolytic activity compared with transferase activity. Substantial conformational changes resulting in an active-site opening were observed, as were changes in the pattern of water molecules bordering the active-site region.

1. Introduction

Sucrose isomerases (SIs; EC 5.4.99.11) belong to glycoside hydrolase family 13 (GH13) in the CAZy classification (Cantarel *et al.*, 2009), which is the major family acting on substrates containing α-glucoside linkages. SIs catalyze the isomerization of sucrose (α-D-glucosylpyranosyl-1,2-β-D-fructofuranose) to trehalulose (α-D-glucosylpyranosyl-1,1-D-fructofuranose) and isomaltulose (α-D-glucosylpyranosyl-1,6-D-fructofuranose) as the main products, and produce glucose and fructose in residual amounts because of sucrose hydrolysis (Fig. 1). They are retaining enzymes and thus there is a net retention of stereochemistry at the anomeric C atom of the product. All GH13 enzymes employ a double-displacement mechanism that involves the formation and breakdown of a covalent glycosyl-enzyme intermediate with an oxocarbenium ion-like transition state (Koshland & Clarke, 1953; Davies & Henrissat, 1995; Mosi *et al.*, 1997; Uitdehaag *et al.*, 1999; Hjerrild *et al.*, 2004). The active site of members of the GH13 family, which contains a large diversity of polysaccharide-metabolizing enzymes and includes over 10 000 enzymes, is composed of a catalytic triad: a catalytic nucleophile, a general acid/base catalyst and a transition-state stabilizer. The catalytic nucleophile attacks the anomeric centre of the sugar, generating the enzyme–substrate intermediate. In a subsequent step, this intermediate undergoes either transglycosylation or hydrolysis. Both steps require the assistance of a general acid/base catalyst and a transition-state stabilizer. Extensive structure–function–activity relationship studies have been undertaken in order to understand the molecular

bases of substrate recognition and transformation in this family, which contains many industrially important enzymes. To date, crystal structures of three SIs have been determined: two isomaltulose synthases, PalI from *Klebsiella* sp. LX3 (Zhang *et al.*, 2003) and SmuA from *Protaminobacter rubrum* (Ravaud *et al.*, 2009), recently renamed *Serratia plymuthica* (Goulter *et al.*, 2012), and one trehalulose synthase, MutB from *Pseudomonas mesoacidophila* MX45 (Ravaud *et al.*, 2007), recently renamed *Rhizobium* sp. (Goulter *et al.*, 2012). SI active sites consist of 14 residues independent of the major product outcome (trehalulose or isomaltulose; Ravaud *et al.*, 2007, 2009). Six of these, including the three essential catalytic residues described above, are conserved within the active sites of other GH13 enzymes (MacGregor *et al.*, 2001), and a further five residues (Asp61, Phe145, Phe164, Gln168 and Arg414; MutB numbering) are conserved in the members of the so-called oligo-1,6-glucosidase subfamily, which includes, amongst others, oligo-1,6-glucosidases and amylosucrases (Oslancová & Janecek, 2002; Ravaud *et al.*, 2007). Another three residues, corresponding to Phe144, Asn328 and Glu386, are specific to sucrose isomerases (Ravaud *et al.*, 2007, 2009; Lipski *et al.*, 2010). Finally, other residues present in the catalytic site (Arg198, Asp384 and Arg284) guide the orientations of the catalytic residues and stabilize the active site (Ravaud *et al.*, 2009). Structural studies performed on complexes of the trehalulose synthase MutB and the isomaltulose synthase SmuA with substrate and substrate analogues indicated that the active site situated in domain A of the three-domain crystal structure displays a pocket shape that is thought to be essential for the isomerization reaction (Ravaud *et al.*, 2007, 2009; Lipski *et al.*, 2010). At the entrance/exit of this pocket, a pair of phenylalanines (Phe256 and Phe280), the so-called aromatic clamp, is believed to play a key role in controlling the reaction specificity by regulating access to and exit from the active site (Ravaud *et al.*, 2007).

Owing to the high transfer activities of MutB (Miyata *et al.*, 1992; Nagai *et al.*, 1994) and SmuA (Weidenhagen, 1957; Tsuyuki *et al.*, 1984; Mattes *et al.*, 1998; Wu & Birch, 2004), biochemical and structural studies of these two enzymes have so far focused on the molecular determinants that are responsible for these transferase activities (see, for example, Zhang *et al.*, 2003; Aroonnual *et al.*, 2007; Cho *et al.*, 2007; Ravaud *et al.*, 2007, 2009; Watzlawick & Mattes, 2009; Görl *et al.*, 2012). In a study of MutB using a random-mutagenesis approach, mutants displaying a major hydrolytic activity emerged (Watzlawick & Mattes, 2009). Two single MutB mutants, R284C and F164L, were selected for biochemical and X-ray crystallographic analyses in order to investigate the molecular and structural bases for the change in catalysis from isomerization to hydrolysis (Fig. 1). Understanding of the factors that govern the increased hydrolytic activity is essential since this activity is highly undesirable in the use of these enzymes in industrial processes for the synthesisis of the sucrose isomers trehalulose and isomaltulose.

Here, we report the characterization of these mutants and their effect on the kinetics of the isomerase activity, as well as the refined three-dimensional structures of the R284C mutant in its free state and of the F164L mutant from crystals soaked in solutions containing substrate and reaction products.

2. Methods

2.1. Protein overexpression and purification

The *mut*B gene variants from *Rhizobium* sp. coding for MutB F164L (*pHWG660.12*) and R284C (*pHWG659.3*) were

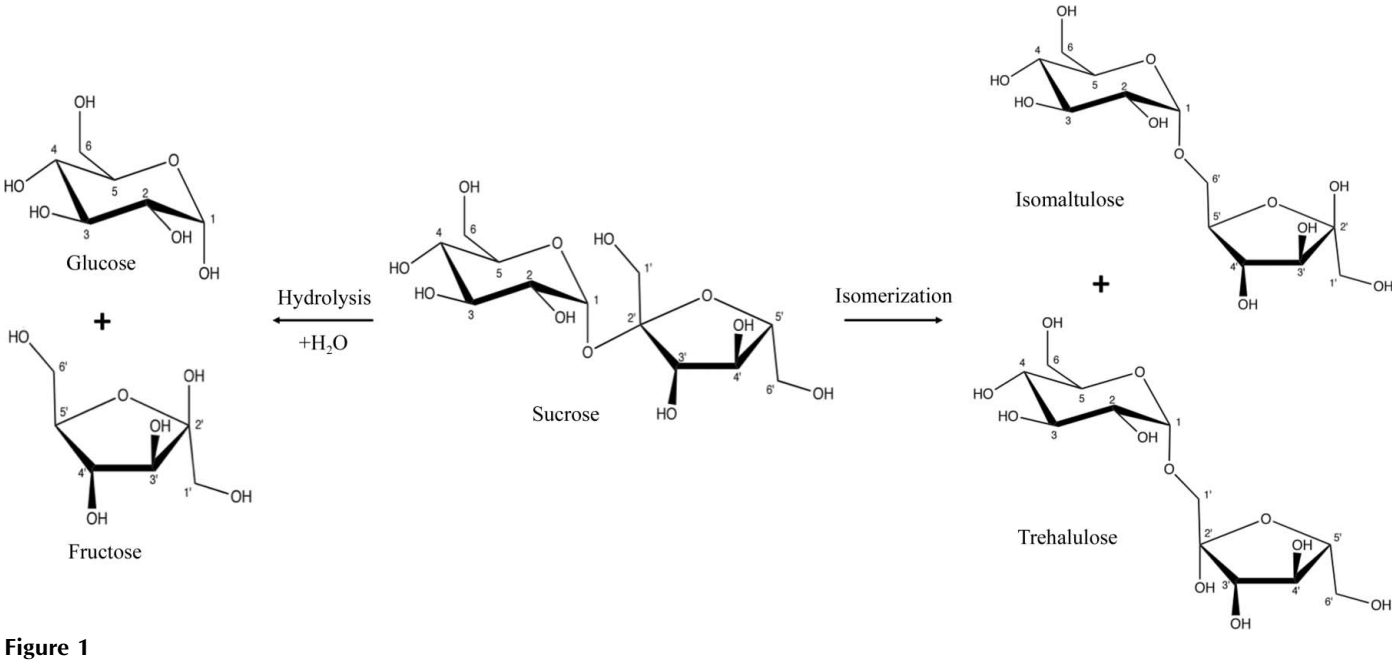

Figure 1
Reactions catalyzed by sucrose isomerases: sucrose is isomerized to isomaltulose and trehalulose as main products (right-hand side of the scheme), but is also hydrolysed to glucose and fructose in trace amounts (left-hand side of the scheme).

Table 1
Data-collection and refinement statistics.

Values in parentheses are for the highest resolution shell.

Mutant	F164L				R284C	
Soaking	Glucose	Sucrose	Trehalulose	Isomaltulose	Deoxynojirimycin	—
Radiation source	ID29, ESRF	ID29, ESRF	ID29, ESRF	ID29, ESRF	BM30A, ESRF	ID14-3, ESRF
Space group	$P2_1$	$P2_1$	$P2_1$	$P2_1$	$P2_12_12_1$	$P2_12_12_1$
Unit-cell parameters						
a (Å)	63.9	64.1	63.9	64.1	83.8	84.1
b (Å)	86.3	86.1	85.9	86.5	89.7	90.1
c (Å)	118.3	118.1	118.7	118.6	91.6	91.6
β (°)	97.9	97.9	97.9	97.7		
Wavelength (Å)	0.97559	0.97559	0.97559	0.97559	0.9699	0.9310
Resolution range (Å)	15.0–2.15	15.0–2.00	15.0–2.15	15.0–2.00	19.9–1.90	16.8–1.70
Completeness (%)	98.5 (98.6)	99.0 (99.5)	95.4 (95.4)	97.1 (81.3)	99.9 (99.9)	99.9 (99.9)
Multiplicity	5.6 (3.5)	7.4 (7.2)	3.2 (3.2)	4.0 (3.9)	4.9 (4.9)	7.4 (7.4)
Total No. of reflections	252093	680844	216681	340191	271600	570047
Unique reflections	66091	68858	84263	55036	55036	77016
$\langle I/\sigma(I)\rangle$	9.4 (3.3)	11.7 (4.0)	8.3 (2.8)	11.1 (3.2)	10.3 (5.4)	9.0 (5.3)
$R_{\rm merge}$† (%)	13.7 (54.0)	13.3 (56.2)	16.5 (55.7)	11.6 (48.8)	11.3 (27.1)	16.3 (44.0)
R factor‡ (%)	17.0	15.8	19.5	16.5	17.4	14.4
$R_{\rm free}$ (%)	21.9	19.3	25.9	21.3	21.1	17.3
R.m.s.d. bond lengths (Å)	0.013	0.013	0.017	0.013	0.008	0.013
R.m.s.d. angles (°)	1.49	1.43	1.64	1.43	1.10	1.43
Average B factor (Å^2)	17.7	15.1	13.7	13.4	13.2	12.0
No. of molecules in the asymmetric unit	2	2	2	2	1	1
No. of atoms						
Water	892	1044	998	1152	716	852
Protein	8984	9098	8962	9015	4505	4572
Ligand	68	92	26	80	24	30
Calcium	2	2	2	2	1	1
Ramachandran statistics (%)						
Favourable	88.2	89.5	87.3	88.9	90.1	90.5
Generously allowed	11.7	10.4	12.6	11.0	9.9	9.3
Additionally allowed	0.1	0.1	0.1	0.1	0.0	0.2
PDB code	4gi6	4gi8	4gi9	4gia	4gin	4h2c

† $R_{\rm merge} = \sum_{hkl}\sum_i |I_i(hkl) - \langle I(hkl)\rangle|/\sum_{hkl}\sum_i I_i(hkl)$, where $I_i(hkl)$ is the intensity of symmetry-related reflections hkl, $\sum_{hkl}$ is the sum over all observations and $\sum_i$ is the sum over i measurements of the reflection. ‡ $R = \sum_{hkl}\big||F_{\rm obs}| - |F_{\rm calc}|\big|/\sum_{hkl}|F_{\rm obs}|$.

obtained after random mutagenesis of *mut*B (pHWG315) in a screening system. After employing a chemical mutagenesis (MNNG) approach on *mut*B, the mutant library was plated on McConkey agar plates supplemented with sucrose. Colonies that displayed a red phenotype, expected to produce more monosaccharides from sucrose, were isolated. Hydrolytic mutants exhibiting the single-amino-acid substitutions R284C and F164L were chosen for further characterization (Watzlawick & Mattes, 2009).

For expression of the genes, the plasmids were transformed in *Escherichia coli* JM109 as described previously (Ravaud, Watzlawick, Haser *et al.*, 2005; Watzlawick & Mattes, 2009), and purification was performed as described for the wild-type enzyme (Watzlawick & Mattes, 2009). Pure enzyme fractions were concentrated to approximately 5 mg ml^{-1} using Amicon devices; the R284C mutant was stored in 10 m*M* calcium acetate buffer pH 5.5, while the F164L mutant was dialysed against 10 m*M* potassium phosphate buffer pH 6.5.

2.2. Crystallization

Crystal growth was performed using the hanging-drop vapour-diffusion technique at 290 K from solutions containing PEG 20 000 as described previously (Ravaud, Watzlawick, Haser *et al.*, 2005; Ravaud *et al.*, 2007). For the F164L mutant, crystals were soaked with trehalulose, isomaltulose, glucose and sucrose for 30 min in crystallization drops to which the respective ligands had been added to a final concentration of 10 m*M*. Crystals of the R284C mutant were soaked with deoxynojirimycin (final concentration of 10 m*M*) for 30 min.

2.3. Data collection and processing

Crystals were cryoprotected prior to data collection by rapid soaking (15 s) in mother liquor containing 20%(*v*/*v*) glycerol. Diffraction data were collected at 100 K using synchrotron radiation on the beamlines of the ESRF in Grenoble as indicated in Table 1. Intensities were integrated and scaled using programs from the *XDS* package (Kabsch, 2010), with the exception of the R284C mutant data, which were reduced using *iMOSFLM* (Battye *et al.*, 2011) and *SCALA* (Evans, 2011). Data-collection statistics are presented in Table 1.

2.4. Structure determination and refinement

The crystal structure obtained from the R284C mutant soaked with deoxynojirymycin was solved by molecular

replacement using the refined MutB–Tris structure at 1.6 Å resolution (PDB entry 1zja; Ravaud *et al.*, 2007) as a search model with the program *AMoRe* (Navaza, 2001). A unique solution was found using diffraction data in the resolution range 15–3.5 Å. The correlation coefficient and *R* factor were 30.8 and 47.4%, respectively. The three-dimensional structure of the R284C mutant in its free state was solved to 1.7 Å resolution using the refined structure of the R284C mutant soaked with deoxynojirimycin as the search model in a molecular-replacement search with the program *Phaser* (McCoy, 2007). After clustering of the rotation-function and translation-function peaks and the purging of peaks below a 75% threshold (default settings in *Phaser*), a single solution emerged with RFZ = 43.5, TFZ = 50.8 and LLG = 5559.

The structures of the F164L mutant complexes were solved by direct phasing using the MutB–Tris structure in the monoclinic form (PDB entry 1zjb; Ravaud, Watzlawick, Mattes *et al.*, 2005), from which Tris had been omitted, to calculate a difference Fourier, which was followed by rigid-body refinement with the program *REFMAC*5 from the *CCP*4 package (Murshudov *et al.*, 2011; Winn *et al.*, 2011). For cross-validation, 5% of the data (for both the R284C and the F164L mutants) were set aside prior to refinement.

Model building and refinement of the F164L mutant structures was performed using *Coot* (Emsley *et al.*, 2010) and *REFMAC*5 (Murshudov *et al.*, 2011), respectively, whereas for the R284C mutant (deoxynojirymycin-soaked) *TURBO-FRODO* (Roussel *et al.*, 1990) and the simulated-annealing protocol in *CNS* (Brünger *et al.*, 1998) were used and the final refinement steps were carried out using *PHENIX* (Adams *et al.*, 2002). For the R284C mutant data (free state) *Coot* (Emsley *et al.*, 2010) and *PHENIX* (Adams *et al.*, 2002) were used for model building and refinement. Based on inspection of $2F_o - F_c$ and $F_o - F_c$ maps (contoured at 1.0σ and 3σ), calcium ions and ligands were inserted and water molecules were added if they had suitable hydrogen-bonding distances and angles to protein atoms or water molecules. Alternative conformations of amino acids were introduced and refined with the appropriate split occupancies when the electron-density maps indicated their presence.

The model quality was assessed using the programs *PROCHECK* (Laskowski, 2001) and *MolProbity* (Chen *et al.*, 2010), and protein and ligand interfaces were analyzed using the *PISA* server (Krissinel & Henrick, 2007) as implemented in the *CCP*4 package.

Superimposition of structures and calculation of the r.m.s.d. between atomic coordinates were carried out using *SUPERPOSE* from the *CCP*4 package (Krissinel & Henrick, 2004) and *DaliLite* (Holm & Park, 2000).

The program *DynDom* (Hayward & Berendsen, 1998) was used to determine dynamic domains, interdomain bending regions and interdomain rotation axes. *DynDom* v.2.0 (http://www.cmp.uea.ac.uk/dyndom/) was used with default parameters.

For the ligands isomaltulose, trehalulose, glucose and sucrose, PDB files and libraries were generated by the *electronic Ligand Builder and Optimization Workbench* (*eLBOW*; Moriarty *et al.*, 2009).

Table 1 summarizes the refinement statistics and model quality.

2.5. Enzyme kinetics

Standard activity tests were performed as described previously (Ravaud, Watzlawick, Haser *et al.*, 2005) using 100 m*M* sucrose as the substrate. After approximately 90% sucrose consumption, the product composition was measured (individual sugars were determined by HPLC as described in Watzlawick & Mattes, 2009). The buffer used for the standard activity test was potassium phosphate pH 6.5 for the F164L mutant. The activity was calculated from the amount of main product produced, where one unit was defined as the formation of 1 µmol of glucose per minute. All reactions were performed in triplicate and the values presented are average values.

Prior to activity measurements, the purified F164L mutant was incubated with sucrose at concentrations ranging from 10 to 200 m*M* under standard assay conditions. Data for the products formed were analyzed using double-reciprocal Lineweaver–Burk plots to calculate the K_m and V_{max} values.

The product composition as a function of temperature was determined from 293 to 323 K after 15 min incubation at the given temperature prior to the addition of sucrose. Analysis of the effect of pH on sucrose isomerase activity was performed using purified enzymes which had been dialysed against 10 m*M* sodium acetate buffer pH 6.5 and then equilibrated in the respective buffer solutions (100 m*M* sodium phosphate pH 5–8).

The effect of metal ions was measured by dialysing the enzymes against 100 m*M* sodium acetate buffer pH 6.5 followed by pre-incubation for 15 min in the presence of 1 m*M* of the respective metal-ion solution. Finally, the effect of glucose on the activity was measured by the stepwise addition of glucose (10, 50 and 100 m*M*) during the standard assay.

The substrate specificity of the mutant enzymes was tested with trehalulose, isomaltulose, trehalose and isomaltose. The activity towards these substrates was measured at 298 K by incubating 45 µl purified enzyme with 5 µl substrate solution at a final concentration of 100 m*M*. The sugar profiles in the reaction mixture were analyzed by HPLC as described above.

2.6. Figure rendering

Figures were generated with the programs *GRASP* (Petrey & Honig, 2003) and *PyMOL* (DeLano, 2002).

2.7. PDB codes

The coordinates and structure factors have been deposited in the Protein Data Bank under entry codes 4h2c (R284C mutant), 4gin (R284C mutant soaked with deoxynojirimycin), 4gi6 (F164L mutant soaked with glucose), 4gi8 (F164L mutant soaked with sucrose), 4gia (F164L mutant soaked with isomaltulose) and 4gi9 (F164L mutant soaked with trehalulose).

3. Results

3.1. Three-dimensional structures of the R284C mutant

The R284C mutant crystals belonged to the orthorhombic space group $P2_12_12_1$, which has never previously been observed for other MutB structures (native, complexes or mutants). The three-dimensional structure of this mutant was solved in a ligand-free state to 1.7 Å resolution with one monomer in the asymmetric unit and revealed a global conformation that was drastically altered compared with the wild-type native structure of MutB, as illustrated by the r.m.s.d. of 1.7 Å between the two structures based on all C^{α} atoms (Fig. 2).

Owing to the mutation of Arg284 to a cysteine, the interaction with the main-chain carbonyl O atom, Asp327 O, is not present in the R284C mutant structure, thus inducing a shift in both the main-chain and the side-chain atoms of Asp327. As a consequence, the salt bridges Asp327 $O^{\delta1}\cdots$Arg414 $N^{\eta1}$, Arg414 $N^{\eta2}\cdots$Asp61 $O^{\delta1}$ and Arg414 $N^{\eta2}\cdots$Asp384 $O^{\delta1}$, which are responsible for the pocket topology of MutB, are disrupted (Fig. 3, Table 2).

This succession of events induces a considerable change in the surroundings of the catalytic pocket and thus of the overall structural conformation, as illustrated in Figs. 2(*a*) and 2(*b*). Analysis of the conformational changes between the R284C mutant and native MutB structures performed using the program *DynDom* (Hayward & Berendsen, 1998) show a well defined domain rotation. More precisely, two domains (1 and 2; shown in red in Fig. 2) are defined as moving domains, whereas one domain is considered as fixed (shown in blue in Fig. 2). The first moving domain is composed of 200 residues covering Nβ2, Nβ2′, Nβ3, Nα3 and the entire subdomain. The second moving domain of 36 residues comprises residues 286–293, 375–380 and 389–410 of the N-terminal catalytic domain. The domains rotate by approximately 10 and 7°, respectively, between the two structures. Two inter-domain bending regions exist (shown in green in Fig. 2). These bending regions are located in the vicinity of the mutated residue and most of them correspond to loop regions (especially the loops between Nα3 and Nβ4, Nβ6 and Nα6, Nα6 and Nβ7, and Nβ8 and Nα8′) and/or to residues that interestingly differ between MutB and the isomaltulose synthases PalI (56, 98, 285, 293–298, 307, 309, 311–313, 315 and 410; MutB numbering) and SmuA (all of the aforementioned residues except 312 and 315).

The crystal structure determined from a crystal soaked with deoxynojirimycin did not show any trace of the ligand in the electron density. The overall structure is identical to that of R284C in its free state, with the exception of the pocket, which is narrower in the structure from the soaked crystals, as

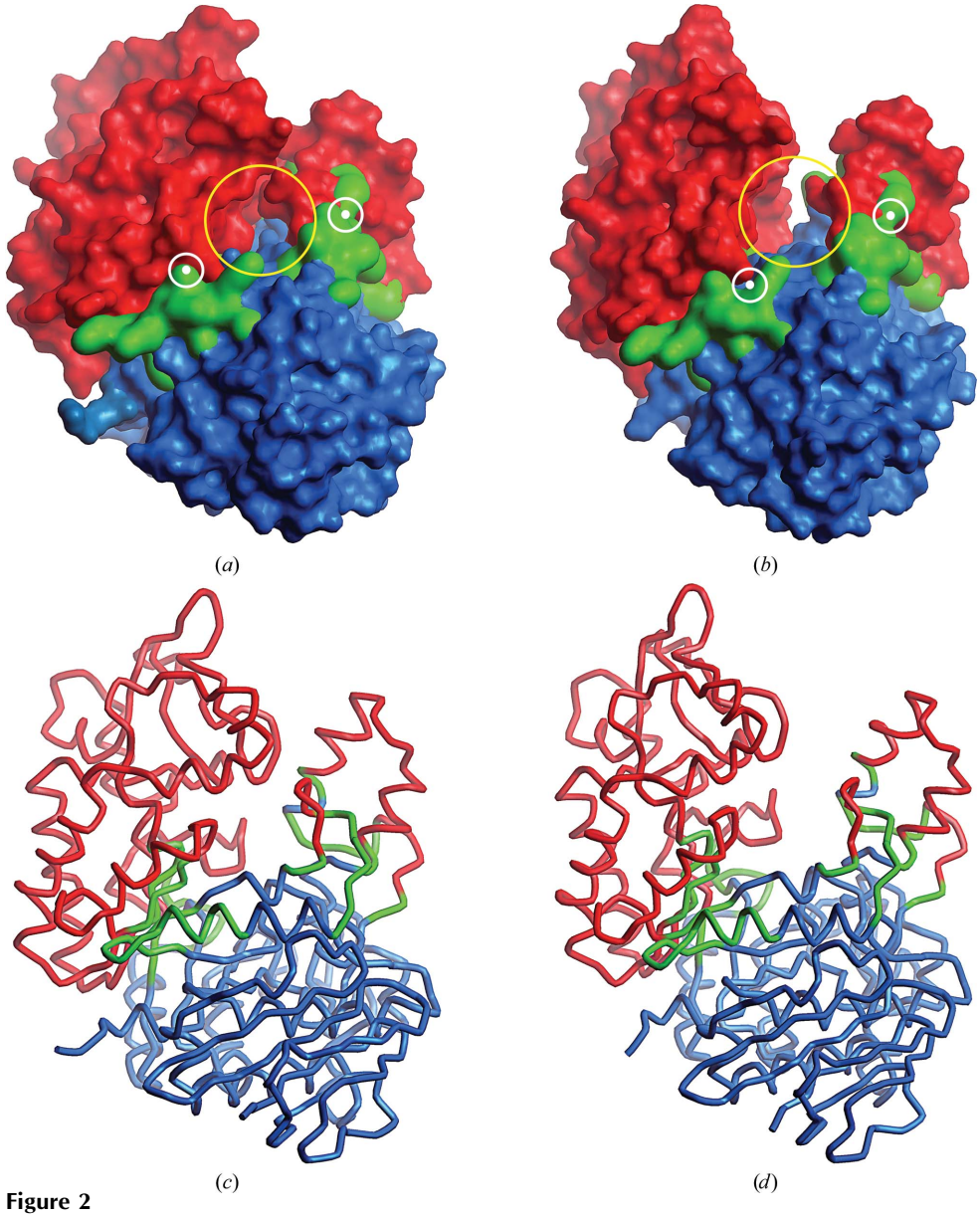

Figure 2
Comparison of the wild-type and R284C mutant MutB structures; the fixed and moving domains (as defined by the *DynDom* program) are coloured blue and red, respectively, and the 'bending' regions are coloured green. The entrance to the catalytic pocket is indicated in yellow and the rotation axes, represented by white circles, are perpendicular to the plane of the paper. (*a*, *b*) Views of the molecular surfaces of the wild-type and mutant R284C MutB structures, respectively. (*c*, *d*) C^{α} traces of the wild-type and R284C mutant MutB structures, respectively, oriented as in (*a*) and (*b*).

Table 2
Distances (Å) between residues in the active site that are crucial for the pocket architecture.

NM: the value was not measurable.

Interacting atoms	Native MutB†	R284C	R284C‡	F164L§
Arg291 $N^{\eta2}\cdots$Phe144 O	2.7	6.4	6.8	27
Arg291 $N^{\eta2}\cdots$Glu386 $O^{\varepsilon2}$	3.0	2.7	3.5	2.9
Arg284 $N^{\eta2}\cdots$Asp327 O	3.2	NM	NM	3.4
Asp327 $O^{\delta1}\cdots$Arg414 $N^{\eta1}$	3.2	5.5	4.1	3.1
Asp327 $O^{\delta1}\cdots$Arg414 $N^{\eta2}$	5.1	3.8	3.3	5.1
Arg414 $N^{\eta2}\cdots$Asp61 $O^{\delta1}$	3.1	7.5	6.0	3.0
Arg414 $N^{\eta2}\cdots$Asp384 $O^{\delta1}$	2.9	5.8	6.7	2.8
Arg414 $N^{\eta1}\cdots$Asp384 $O^{\delta2}$	5.0	2.9	4.7	4.9
Asp200 $O^{\delta1}\cdots$Arg198 $N^{\eta1}$	3.0	2.7	2.7	3.2

† Values from the crystal structure of native MutB (Ravaud *et al.*, 2007). ‡ Structure of R284C mutant crystals soaked with deoxynojirimycin. § Structure of F164L mutant crystals soaked with glucose.

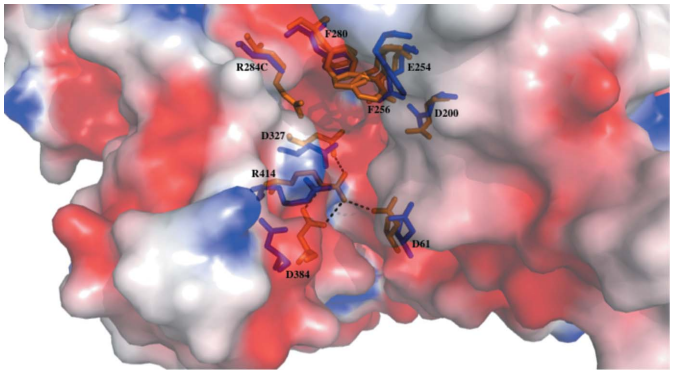

Figure 3
Close-up of the catalytic pocket. Side chains of residues involved in salt bridges defining the catalytic pocket are shown as sticks (in orange for wild-type MutB and in dark blue for the R284C mutant structure) and interactions are shown as dotted lines. The molecular surface of the R284C mutant highlighting the opening of the active site to a cleft is coloured as a function of the electrostatic potential (red, negative charge; blue, positive charge).

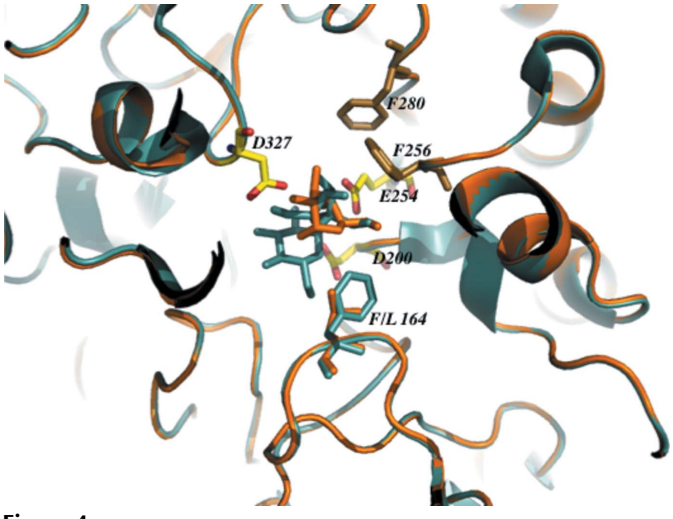

Figure 4
Close-up of the active site with glucose bound in subsite +1 in the F164L mutant (this study; orange) compared with subsite −1 in the inactive E254Q mutant–sucrose complex (light teal; Ravaud *et al.*, 2007). The mutated residue (F164L) is highlighted.

observed from the altered distances between Arg414 and Asp61 in the two R284C mutant structures (Table 2).

3.2. Three-dimensional structures of the F164L mutant

Three-dimensional structures of the F164L mutant were solved at 2.0, 2.15, 2.0 and 2.15 Å resolution using crystals soaked in solutions containing isomaltulose (reaction product), trehalulose (reaction product), sucrose (substrate) and glucose (inhibitor of the native enzyme), respectively. All F164L mutant crystals belonged to the monoclinic space group $P2_1$ and contained two monomers in the asymmetric unit. The overall structure of this mutant is similar to that of the native enzyme (Ravaud *et al.*, 2007), with r.m.s.d.s of 0.3, 0.2, 0.2 and 0.2 Å, respectively, for the structures described above. In the crystal structure of the catalytic acid/base knockout mutant of MutB (E254Q mutant) in complex with sucrose, the phenylalanine (residue 164) has been shown to be part of the bottom/floor of the active-site pocket, where it makes stacking inter-

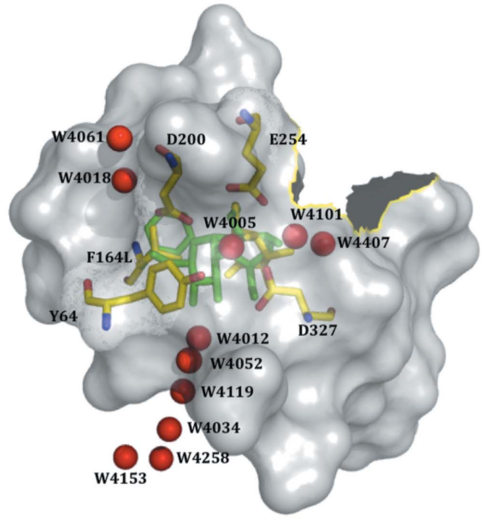

(*a*)

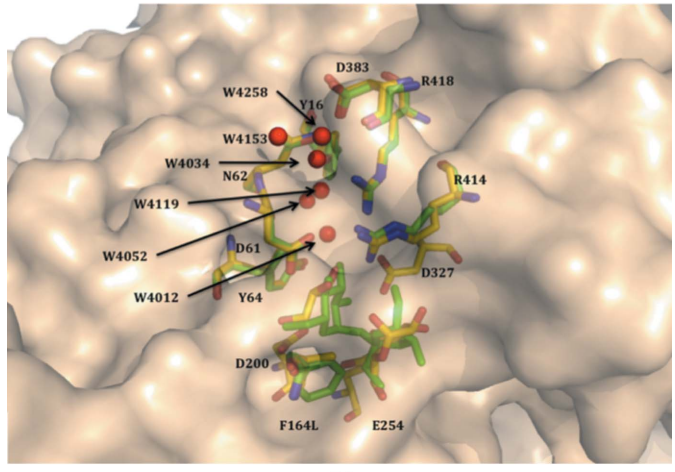

(*b*)

Figure 5
(*a*) Chains of water molecules bordering the active site. (*b*) Partial surface representation of the overall structure of F164L–glucose with water molecules appearing at the surface (Wat4153 and Wat4258) and passing through the enzyme to the active site.

Table 3
Product composition after 90% sucrose consumption (mol% at 298 K) of MutB enzymes in different enzyme buffers.

NR: value not reported.

	Trehalulose	Isomaltulose	Glucose	Fructose	Monosaccharides
Native MutB					
Calcium acetate buffer†	85.3 ± 0.9	13.6 ± 0.9	NR	NR	0.9 ± 0.3
F164L					
Calcium acetate buffer†	30.3 ± 1.0	21.1 ± 1.1	NR	NR	48.0 ± 2.2
Potassium phosphate buffer	24.6 ± 1.1	27.4 ± 1.6	23.8 ± 0.8	24.2 ± 0.7	48.0 ± 1.5
R284C					
Calcium acetate buffer†	15.5 ± 1.5	5.0 ± 1.0	NR	NR	79.0 ± 1.4
Potassium phosphate buffer	43.6 ± 1.6	10.3 ± 0.7	22.3 ± 1.0	23.8 ± 1.1	46.1 ± 2.2

† The measurements in calcium acetate buffer are from Watzlawick & Mattes (2009).

Table 4
Kinetic parameters for the hydrolytic MutB enzymes.

	K_m (m*M*)	V_{max} (U mg^{-1})	k_{cat} (s^{-1})	k_{cat}/K_m (M^{-1} s^{-1})	Reference
R284C/glucose	43	31	32.5	760	Watzlawick & Mattes (2009)
F164L/glucose	75	4	4.2	56	This work

actions with the glucose moiety of the substrate in subsite −1 (Ravaud *et al.*, 2007; Lipski *et al.*, 2010). Inspection of the electron densities of the F164L mutant structures revealed that only the structure obtained from crystals soaked with glucose displays a glucose moiety in one of the two molecules of the structure (molecule *A*), in which it occupies subsite +1 (Fig. 4). In this crystal structure a glycerol molecule is present in subsite −1, in which O1, O2 and O3 of glycerol mimic the positions of hydroxyl groups O3, O4 and O6, respectively, of the glucose moiety in the sucrose molecule of the E254Q–sucrose complex (Fig. 4). Moreover, a water molecule (Wat4005) mimics O2 of the glucose moiety. In molecule *B* a Tris molecule and a glycerol molecule are present in the active site (not shown). Structures determined from crystals soaked in sucrose, trehalulose and isomaltulose showed either both Tris and glycerol molecules or two glycerol molecules in the active site, again with hydroxyl groups mimicking the positions of the O atoms of the disaccharide ligands, as observed for a number of glycoside hydrolases (Aghajari *et al.*, 1998; Skov *et al.*, 2001; Vandermarliere *et al.*, 2009). Attempts to avoid the binding of Tris to the active site by using crystallization conditions lacking Tris, as described for the native enzyme (Ravaud *et al.*, 2007), remained unsuccessful. In the three-dimensional structure of the F164L mutant with glucose bound to the active site, several 'chains' of water molecules are identified adjacent to the active-site pocket (Fig. 5). Of these, two seem to be particularly suited for participation in the hydrolytic reaction. One is made up of two water molecules, Wat4101 and Wat4407, which are present in all of the crystal structures of MutB that have been solved to date. Wat4101, the putative catalytic water molecule pointing towards the scissile bond, forms hydrogen bonds to Asn325 and two of the three catalytic residues, Asp327 (the transition-state stabilizer) and Glu254 (the general acid/base catalyst). The second water chain (Wat4012, Wat4119, Wat4034, Wat4258 and Wat4153) is partly conserved in the sucrose-bound inactive enzyme. The appearance of Wat4258 and Wat4153 in the F164L–glucose structure ensures the connection of the remaining waters from the surface of the enzyme to subsite −1 of the catalytic pocket.

3.3. Enzymatic characterization

The product profiles at 298 K for the two hydrolytic MutB mutants are summarized in Table 3 and the kinetic data are summarized in Table 4. The reaction products of the R284C and F164L mutants with 100 m*M* sucrose at 298 K were predominantly the monosaccharides glucose and fructose (Table 3) and they can therefore be considered to be hydrolytic mutants. For the R284C mutant in calcium acetate and potassium phosphate buffers the product compositions were 79% and 46% monosaccharides, respectively; while the product for the F164L mutant contained 48% monosaccharides independent of the buffer composition. Interestingly, monosaccharide production by the R284C mutant is pH-dependent, with a maximum amount of monosaccharides being produced at low pH. The catalytic efficiency of the F164L mutant was approximately eight times lower than that of the R284C mutant.

3.4. Effect of temperature, pH, metal ions and glucose on the enzymatic activity

The R284C mutant in potassium phosphate buffer pH 6.5 produces mainly monosaccharides in the temperature range 303–333 K and clearly shows a temperature dependence, with the formation of isomers and in particular trehalulose at 293 K (Fig. 6*a*). Moreover, this variant displayed a pH dependence, with the maximum amount of monosaccharides being formed at pH values below pH 6 and a stepwise increase in the amount of trehalulose that was formed with increasing pH (Fig. 6*c*). For the F164L mutant, a 1:1 molar ratio of isomerization products (trehalulose and isomaltulose) and monosaccharides was formed in the temperature range 283–298 K (Fig. 6*b*), whereas between 303 and 313 K the molar ratio of monosaccharides to isomerization products was 3:1. The activity diminished significantly above 313 K and was completely abolished at 318 K. The ratio of sucrose isomers formed by this mutant is less pH dependent; the overall activity diminished significantly at pH values above 6.5 and the mutant became totally inactive at pH 8 (Fig. 6*d*). The F164L mutant is less resistant to temperature changes than the other hydrolytic mutant (R284C).

Activity measurements in the presence of Mg^{2+}, Ca^{2+} and Zn^{2+} ions and of glucose indicated that none of these had any effect on the activity of the R284C mutant (data not shown).

3.5. Substrate specificity

Studies of *S. plymuthica* ATCC 15928 sucrose isomerase demonstrated the use of isomaltulose as a substrate for the production of trehalulose, glucose and fructose (Veronese & Perlot, 1998), whereas purified MutB is highly specific for the substrate sucrose (α-D-glucopyranosyl-1,2-β-D-fructofuranoside; Ravaud, Watzlawick, Haser *et al.*, 2005; Watzlawick & Mattes, 2009). Activity assays with the hydrolytic mutants using trehalulose (α-D-glucopyranosyl-1,1-D-fructose), isomaltulose (α-D-glucopyranosyl-1,6-D-fructofuranose), trehalose (α-D-glucopyranosyl-1,1-α-D-glucopyranoside) and isomaltose (α-D-glucopyranosyl-1,6-α-D-glucopyranoside) as substrates indicated a behaviour similar to that of the native enzyme (data not shown).

4. Discussion

The opening of the active-site pocket of the hydrolytic R284C mutant changes the active-site conformation to the cleft typical of hydrolytic GH13 enzymes, as observed in the structures of α-amylases and other hydrolytic enzymes such as, for example, limit dextrinase (Robert *et al.*, 2005; Vester-Christensen *et al.*, 2010). This opening, which results from the movement of domains 1 and 2 and which allows access of water molecules to the active site, as well as a local structural rearrangement of Phe256 (one of the aromatic clamp residues described previously; Ravaud *et al.*, 2007), favours (along with higher temperatures) the formation of monosaccharides. This drastic domain movement provides strong structural evidence that the pocket architecture is essential for promoting isomerase activity. Despite the fact that the other hydrolytic mutant studied, F164L, has the same phenotype, no drastic changes were observed in the catalytic domain. Since hydrolytic activity necessarily involves water molecules, comparative studies of the water molecules in all known structures of MutB were performed. The results highlighted the presence of a water channel in all of the structures of MutB, both native and mutant, but not in the R284C mutant. Indeed, in the R284C mutant structure residues Asp61, Arg418 and Ile385, which are involved in direct hydrogen bonds to water molecules from the channel, are located in the moving domain, in the fixed domain and in the bending region, respectively. We have previously hypothesized that this water channel serves to refill the catalytic pocket with water (Ravaud *et al.*, 2008). The binding of glucose to the active site of the F164L–glucose complex seems to have induced ordering of water molecules at the surface, where Wat4258 and Wat4153 join the aforementioned conserved water channel. As a consequence, this channel constitutes a water-molecule pathway linking the bulk solvent to the active site. The F164L mutation has therefore induced a new entry allowing water molecules to access the active site *via* subsite −1 and to approach the covalent reaction intermediate owing to the reduced size of the leucine side chain compared with that of phenylalanine. In contrast, the nonmutated enzyme only seems to be accessible *via* the entry at the aromatic clamp level. Within this water channel, Wat4012 (Figs. 5*a* and 5*b*), which is observed in all of the structures with a pocket-formed active site and is located at the bottom of the pocket close to the substrate, is approxi-

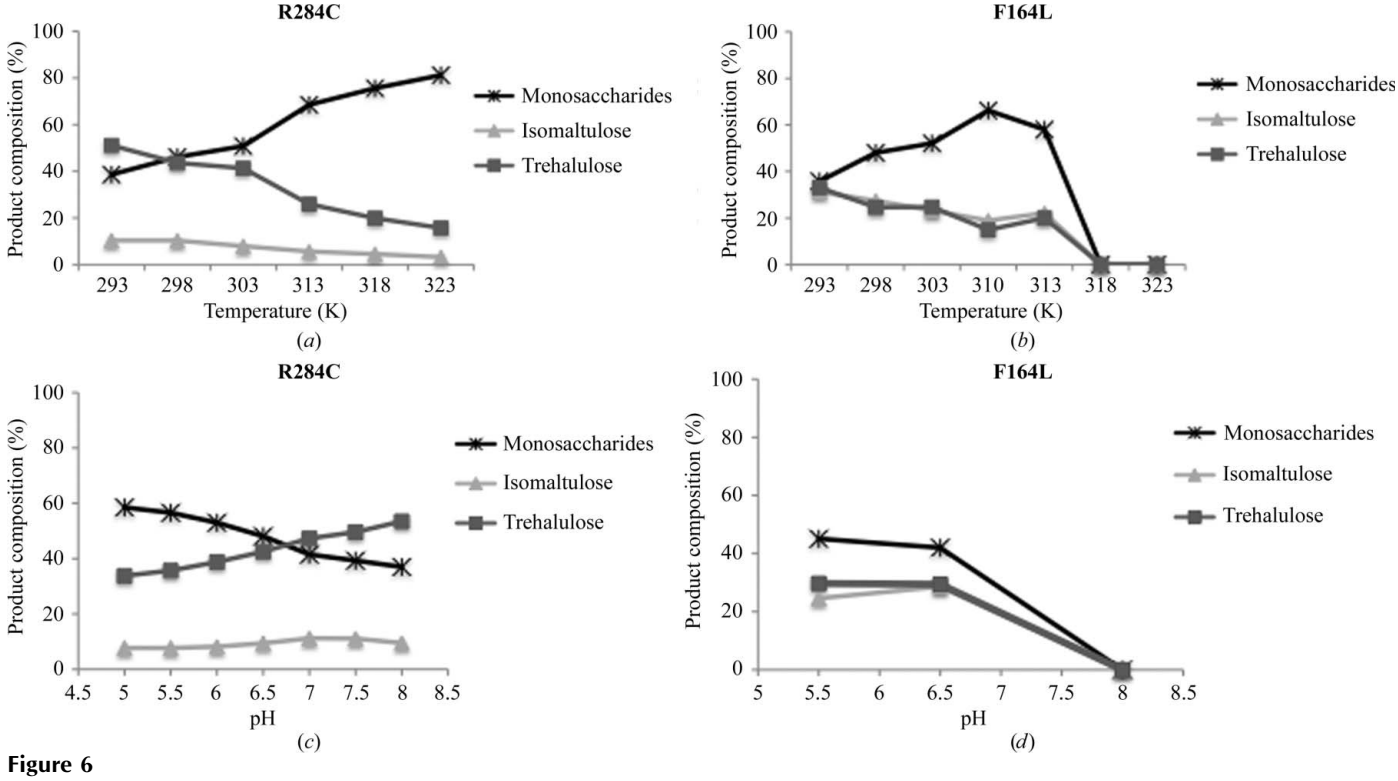

Figure 6
Effect of temperature (*a*) and (*b*) and of pH (*c*) and (*d*) on the product composition of the R284C and F164L mutants.

mately 7.5 Å from the putative covalent glucosyl-enzyme bond and cannot be considered to be the catalytic water in the hydrolytic process. It should be noted that when the native enzyme is bound to its substrate (Ravaud *et al.*, 2007), Wat4012 is implicated in substrate binding by mediating the interactions of O4 and O3 of the glucosyl ring of the sucrose with three residues (Asp61, Arg414 and Arg418). The non-optimal position of this channel for hydrolysis, as well as the aromatic clamp residues possibly obstructing the exit of the newly formed monosaccharide from the active site, is in excellent agreement with the relatively weak hydrolytic activity of the enzyme compared with more optimized systems in which the active site is continuously and efficiently supplied with water (Boel *et al.*, 1990; Aghajari *et al.*, 1998). These latter systems mainly display an inner water pocket containing several solvent molecules and/or a water channel joining the surface of the enzyme to the active site, in which the catalytic water points directly towards the scissile bond.

Activity studies also indicated that the hydrolytic activity of the F164L mutant is lower than that of the other hydrolytic mutant R284C (Table 4). The greater hydrolytic activity of the latter mutant is in agreement with the active site being more open, resulting in increased traffic of molecules entering and exiting the active site. The enzyme products are strongly dependent on the temperature and on the pH, with an increased amount of monosaccharides generally being formed at high temperatures. This is probably owing to the lability of the fructose moiety of the substrate sucrose in the active site, which was previously shown to bind to subsite +1 (Ravaud *et al.*, 2007), being increased at higher temperatures, together with higher mobility of the sugar moieties in general owing to the increased temperature. In the F164L variant, besides inducing a new entry for water molecules, the mutation in subsite −1 partly obstructs stacking interactions with the sugar residue. Indeed, the crystal structures of complexes of MutB (native as well as variant) have shown that the side chain of Phe164, amongst others, mediates the binding of the glucose moiety of the substrate to the enzyme in a stacking interaction (Ravaud *et al.*, 2007). The inactivation of F164L at higher temperatures may be a consequence of this weakened substrate binding combined with increased dynamics of the active-site residues.

In the case of another hydrolytic enzyme, the sucrose hydrolase SUH from *Xanthomonas axonopodis* pv. *glycines*, it has been shown that binding of the substrate sucrose to the catalytic site induces a pocket-shaped active site similar to that found in MutB and other sucrose isomerases, although it only displays hydrolytic activity (Kim *et al.*, 2008). In a homologous sucrose hydrolase from *X. campestris* pv. *campestris* for which the crystal structure was solved in an unliganded form (Champion *et al.*, 2009), the active site is open as observed here for the hydrolytic R284C MutB mutant. Interestingly, it was noticed that residues Arg516 and Asp138 (corresponding to Arg414 and Asp61 in MutB), which form a salt bridge in the *X. axonopodis* sucrose complex and which define part of the glucosyl-binding determinants in subsite −1, were not engaged in salt-bridge formation in the resting *X. campestris* enzyme. With the missing salt bridge an opening was created, resulting in access to subsite −1 from the nonreducing end (Champion *et al.*, 2009). The authors concluded that the binding of a glucosyl moiety in subsite −1 probably induced changes in the conformation of the active-site cleft of the *X. campestris* enzyme. In MutB, Arg414 and Asp61 are among the residues that are essential for the pocket architecture and the disruption of the salt bridge involving these two residues as a consequence of the R284C mutation clearly contributes to conferring hydrolytic activity to the MutB mutant enzyme. An attempt to bind the transition-state mimic deoxynojirimycin to the active site of hydrolytic R284C mutant crystals in a soaking experiment, in order to determine whether the binding could induce a conformation approaching the pocket form, was unsuccessful. Nevertheless, this seems to have influenced the conformation of the pocket to a smaller extent, as observed from the altered distances between Arg414 and Asp61 and Asp384, respectively, in the two R284C mutant structures (Table 2). Whether this is owing to deoxynojirimycin being present in the active site but only with weak occupancy or to deoxynojirimycin replacing cryoprotectant molecules remains uncertain.

Overall, the structural studies and biochemical characterization of the sucrose isomerase hydrolytic mutants presented here have contributed to confirming previous hypotheses on the importance of the pocket geometry of the active site for the isomerization reaction. Furthermore, our studies have revealed the residues that are crucial for this active-site architecture, as well as for substrate binding, and thereby provide new insights into our understanding of the functioning of these important industrial enzymes.

This work was supported by the CNRS – French National Center for Scientific Research (PhD grant to AL) and by the University of Lyon 1. We acknowledge access to beamlines FIP BM30A, ID14-3 and ID29 at the European Synchrotron Radiation Facility (ESRF, Grenoble, France) and the excellent support of the beamline scientists.

References

Adams, P. D., Grosse-Kunstleve, R. W., Hung, L.-W., Ioerger, T. R., McCoy, A. J., Moriarty, N. W., Read, R. J., Sacchettini, J. C., Sauter, N. K. & Terwilliger, T. C. (2002). *Acta Cryst.* D**58**, 1948–1954.

Aghajari, N., Feller, G. & Gerday, C. (1998). *Protein Sci.* **7**, 7564–7572.

Aroonnual, A., Nihira, T. & Seki, T. (2007). *Enzyme Microb. Technol.* **40**, 1221–1227.

Battye, T. G. G., Kontogiannis, L., Johnson, O., Powell, H. R. & Leslie, A. G. W. (2011). *Acta Cryst.* D**67**, 271–281.

Boel, E., Brady, L., Brzozowski, A. M., Derewenda, Z., Dodson, G. G., Jensen, V. J., Petersen, S. B., Swift, H., Thim, L. & Woldike, H. F. (1990). *Biochemistry*, **29**, 6244–6249.

Brünger, A. T., Adams, P. D., Clore, G. M., DeLano, W. L., Gros, P., Grosse-Kunstleve, R. W., Jiang, J.-S., Kuszewski, J., Nilges, M., Pannu, N. S., Read, R. J., Rice, L. M., Simonson, T. & Warren, G. L. (1998). *Acta Cryst.* D**54**, 905–921.

Cantarel, B. L., Coutinho, P. M., Rancurel, C., Bernard, T., Lombard, V. & Henrissat, B. (2009). *Nucleic Acids Res.* **37**, D233–D238.

Champion, E., Remaud-Simeon, M., Skov, L. K., Kastrup, J. S., Gajhede, M. & Mirza, O. (2009). *Acta Cryst.* D**65**, 1309–1314.

Chen, V. B., Arendall, W. B., Headd, J. J., Keedy, D. A., Immormino, R. M., Kapral, G. J., Murray, L. W., Richardson, J. S. & Richardson, D. C. (2010). *Acta Cryst.* D**66**, 12–21.
Cho, M.-H., Park, S.-E., Lim, J. K., Kim, J.-S., Kim, J. H., Kwon, D. Y. & Park, C.-S. (2007). *Biotechnol. Lett.* **29**, 453–458.
Davies, G. & Henrissat, B. (1995). *Structure*, **3**, 853–859.
DeLano, W. L. (2002). *PyMOL*. http://www.pymol.org.
Emsley, P., Lohkamp, B., Scott, W. G. & Cowtan, K. (2010). *Acta Cryst.* D**66**, 486–501.
Evans, P. R. (2011). *Acta Cryst.* D**67**, 282–292.
Görl, J., Timm, M. & Seibel, J. (2012). *Chembiochem*, **13**, 149–156.
Goulter, K. C., Hashimi, S. M. & Birch, R. G. (2012). *Enzyme Microb. Technol.* **50**, 57–64.
Hayward, S. & Berendsen, H. J. (1998). *Proteins*, **30**, 144–154.
Hjerrild, M., Stensballe, A., Jensen, O. N., Gammeltoft, S. & Rasmussen, T. E. (2004). *FEBS Lett.* **568**, 55–59.
Holm, L. & Park, J. (2000). *Bioinformatics*, **16**, 566–567.
Kabsch, W. (2010). *Acta Cryst.* D**66**, 125–132.
Kim, M.-I., Kim, H.-S., Jung, J. & Rhee, S. (2008). *J. Mol. Biol.* **380**, 636–647.
Koshland, D. E. & Clarke, E. (1953). *J. Biol. Chem.* **205**, 917–924.
Krissinel, E. & Henrick, K. (2004). *Acta Cryst.* D**60**, 2256–2268.
Krissinel, E. & Henrick, K. (2007). *J. Mol. Biol.* **372**, 774–797.
Laskowski, R. A. (2001). *Nucleic Acids Res.* **29**, 221–222.
Lipski, A., Rhimi, M., Haser, R. & Aghajari, N. (2010). *J. Appl. Glycosci.* **57**, 219–228.
MacGregor, E. A., Janecek, S. & Svensson, B. (2001). *Biochim. Biophys. Acta*, **1546**, 1–20.
Mattes, R., Klein, K., Schiweck, H., Kunz, M. & Munir, M. (1998). US Patent 5786140.
McCoy, A. J. (2007). *Acta Cryst.* D**63**, 32–41.
Miyata, Y., Sugitani, T., Tsuyuki, K., Ebashi, T. & Nakajima, Y. (1992). *Biosci. Biotechnol. Biochem.* **56**, 1680–1681.
Moriarty, N. W., Grosse-Kunstleve, R. W. & Adams, P. D. (2009). *Acta Cryst.* D**65**, 1074–1080.
Mosi, R., He, S., Uitdehaag, J., Dijkstra, B. W. & Withers, S. G. (1997). *Biochemistry*, **36**, 9927–9934.
Murshudov, G. N., Skubák, P., Lebedev, A. A., Pannu, N. S., Steiner, R. A., Nicholls, R. A., Winn, M. D., Long, F. & Vagin, A. A. (2011). *Acta Cryst.* D**67**, 355–367.
Nagai, Y., Sugitani, T. & Tsuyuki, K. (1994). *Biosci. Biotechnol. Biochem.* **58**, 1789–1793.
Navaza, J. (2001). *Acta Cryst.* D**57**, 1367–1372.
Oslancová, A. & Janecek, S. (2002). *Cell. Mol. Life Sci.* **59**, 1945–1959.
Petrey, D. & Honig, B. (2003). *Methods Enzymol.* **374**, 492–509.
Ravaud, S., Robert, X., Watzlawick, H., Haser, R., Mattes, R. & Aghajari, N. (2007). *J. Biol. Chem.* **282**, 28126–28136.
Ravaud, S., Robert, X., Watzlawick, H., Haser, R., Mattes, R. & Aghajari, N. (2009). *FEBS Lett.* **583**, 1964–1968.
Ravaud, S., Robert, X., Watzlawick, H., Laurent, S., Haser, R., Mattes, R. & Aghajari, N. (2008). *Biocatal. Biotransformation*, **26**, 111–119.
Ravaud, S., Watzlawick, H., Haser, R., Mattes, R. & Aghajari, N. (2005). *Acta Cryst.* F**61**, 100–103.
Ravaud, S., Watzlawick, H., Mattes, R., Haser, R. & Aghajari, N. (2005). *Biologia*, **60**, 89–95.
Robert, X., Haser, R., Mori, H., Svensson, B. & Aghajari, N. (2005). *J. Biol. Chem.* **280**, 32968–32978.
Roussel, A., Fontecilla-Camps, J. C. & Cambillau, C. (1990). *J. Mol. Graph.* **8**, 86–91.
Skov, L. K., Mirza, O., Henriksen, A., De Montalk, G. P., Remaud-Simeon, M., Sarçabal, P., Willemot, R. M., Monsan, P. & Gajhede, M. (2001). *J. Biol. Chem.* **276**, 25273–25278.
Tsuyuki, K., Sugitani, T., Miyata, Y., Ebashi, T., Yakajima, T. & Miyata, T. (1984). *Caries Res.* **18**, 47–51.
Uitdehaag, J. C., Mosi, R., Kalk, K. H., van der Veen, B. A., Dijkhuizen, L., Withers, S. G. & Dijkstra, B. W. (1999). *Nature Struct. Biol.* **6**, 432–436.
Vandermarliere, E., Bourgois, T. M., Winn, M. D., van Campenhout, S., Volckaert, G., Delcour, J. A., Strelkov, S. V., Rabijns, A. & Courtin, C. M. (2009). *Biochem. J.* **418**, 39–47.
Veronese, T. & Perlot, P. (1998). *FEBS Lett.* **441**, 348–352.
Vester-Christensen, M. B., Abou Hachem, M., Svensson, B. & Henriksen, A. (2010). *J. Mol. Biol.* **403**, 739–750.
Watzlawick, H. & Mattes, R. (2009). *Appl. Environ. Microbiol.* **75**, 7026–7036.
Weidenhagen, R.(1957). *Chem. Ber.* **90**, 1046–1050.
Winn, M. D. *et al.* (2011). *Acta Cryst.* D**67**, 235–242.
Wu, L. & Birch, R. G. (2004). *J. Appl. Microbiol.* **97**, 93–103.
Zhang, D., Li, N., Lok, S.-M., Zhang, L.-H. & Swaminathan, K. (2003). *J. Biol. Chem.* **278**, 35428–35434.